ACS Macro Letters

Letter

pubs.acs.org/macroletters

Simple Route for Tuning the Morphology and Conductivity of Polymer Electrolytes: One End Functional Group is Enough

Gyuha Jo,[†] Hyungmin Ahn,[†] and Moon Jeong Park*[,†,‡]

[†]Department of Chemistry and [‡]Division of Advanced Materials Science (WCU), Pohang University of Science and Technology (POSTECH), Pohang, Korea 790-784

Supporting Information

ABSTRACT: We have investigated a new means to control the morphology and conductivity of block copolymer electrolytes by the inclusion of ionic units at the chain ends. A set of poly(styrene-*b*-ethylene oxide) (PS-b-PEO) block copolymers having dissimilar PEO end groups (−OH, $-SO_3H$, and $-SO_3Li$) exhibited various self-assembled morphologies including disordered, lamellar, and hexagonal cylindrical phases. Strikingly, the addition of Li salts to PS-b-PEO with sulfonate terminal groups afforded enriched nanostructures with significant differences in their conductivities depending on the salt concentration. In particular, a gyroid morphology with a 2-fold-enhanced normalized ionic conductivity was found for the sulfonate-terminated PS-b-PEO when compared to disordered PS-b-PEO-OH. This is closely related to the structural advantages of gyroid having cocontinuous ionic channels, which enable efficient transport of Li^+ ions via less tortuous ion conduction pathways. This work presents fascinating experimental insights on the enhancement of ion transport efficiencies by modulating the self-assembly nature of polymer electrolytes by substituting with a single end-functional group.

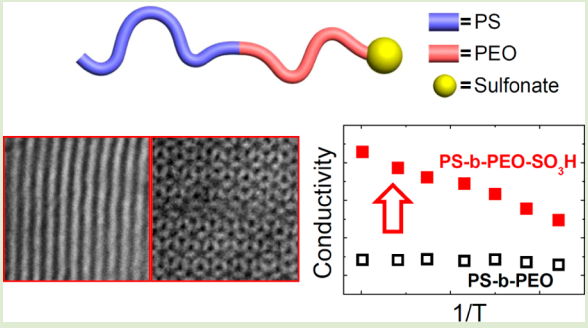

Since the discovery of ionic conductivity in poly(ethylene oxide) (PEO) doped with sodium in 1975,[1] PEO and lithium salt complexes have remained long-standing candidates for lithium battery electrolytes.[2] In recent years, as the realization of high mechanical strength from polymer electrolytes becomes of critical importance in high-energy lithium batteries,[3−5] a wide variety of strategies to synthesize new polymer electrolytes comprising PEO chains and mechanically robust polymers have been proposed.[3−7]

Particularly, the creation of polymer electrolytes possessing phase-separated morphologies by designing them in block,[3−7] graft,[8] and dendrimer[9,10] configurations has been the subject of extensive studies in order to establish a synergistic means of optimizing Li^+ transport rates and mechanical integrity. Interest in this topic has been further stimulated by multiple observations of significant electrolytic conductivity enhancement imparted by particular nanoscale morphologies.[11,12] The block architecture is most widely utilized in the construction of desired nanostructures with improved transport properties owing to a well-established experimental and theoretical background on the thermodynamics of block copolymers spanning decades of research.[13]

There exist several reports on the successful morphological tuning of PEO-containing block copolymers using a number of synthetic strategies.[14−16] The most commonly employed method is the variation of molecular weights and compositions of constituent blocks;[14,15] however, the difficulties in correlating morphological effects on conductivity arises from the fact that the different molecular weights and compositions of block copolymers themselves also influence ion diffusion coefficients, which are tied to ion transport properties.[5,17] Elucidation of the morphology−conductivity relationship has thus been accompanied by arithmetic methods, primarily taking into account the segmental motion of polymer chains and the volume of conducting phases.[18,19] Nevertheless, conclusions to these longstanding issues remain controversial.[11,18−21]

Quantitative analysis of the link between morphology and conductivity could be simplified if one can tune the morphology of block copolymer electrolytes through unconventional means. This involves the incorporation of end functional units into the polymer chains while maintaining other chemical functionality intact.[22] In fact, there are a significant number of studies that show the effects of terminal groups on the physicochemical properties of polymers; however, most approaches have been limited to solutions (micelle),[23] thin films (surface properties),[24] and reactive homopolymer mixtures.[25] The development of organic electronic devices using bulk polymers bearing functional substituents has attracted considerable attention recently,[26] but the knowledge to tailor their self-assembly properties using embedded functionality is still significantly lacking.

Herein, we report a method for the precise control over nanoscale morphology of polymer electrolytes by means of

Received: September 6, 2013
Accepted: October 18, 2013
Published: October 22, 2013

 © 2013 American Chemical Society dx.doi.org/10.1021/mz400468m | *ACS Macro Lett.* 2013, 2, 990−995

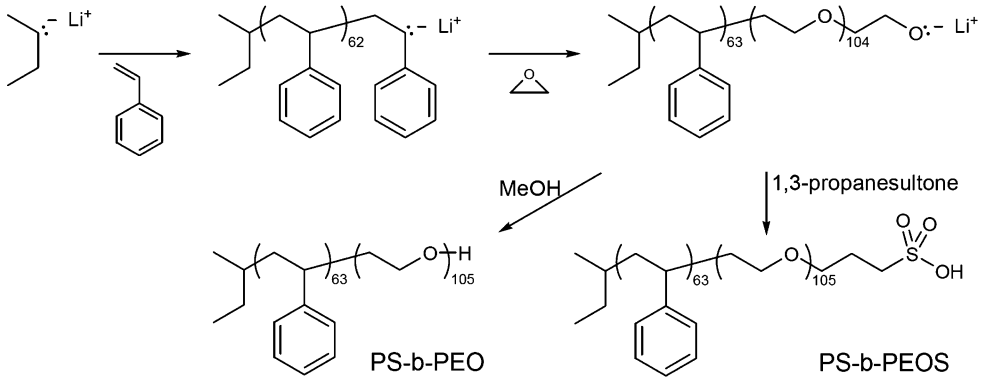

Figure 1. Synthetic procedures of PS-b-PEO block copolymers having dissimilar end groups: (a) alcohol (−OH) and (b) sulfonic acid ($-SO_3H$).

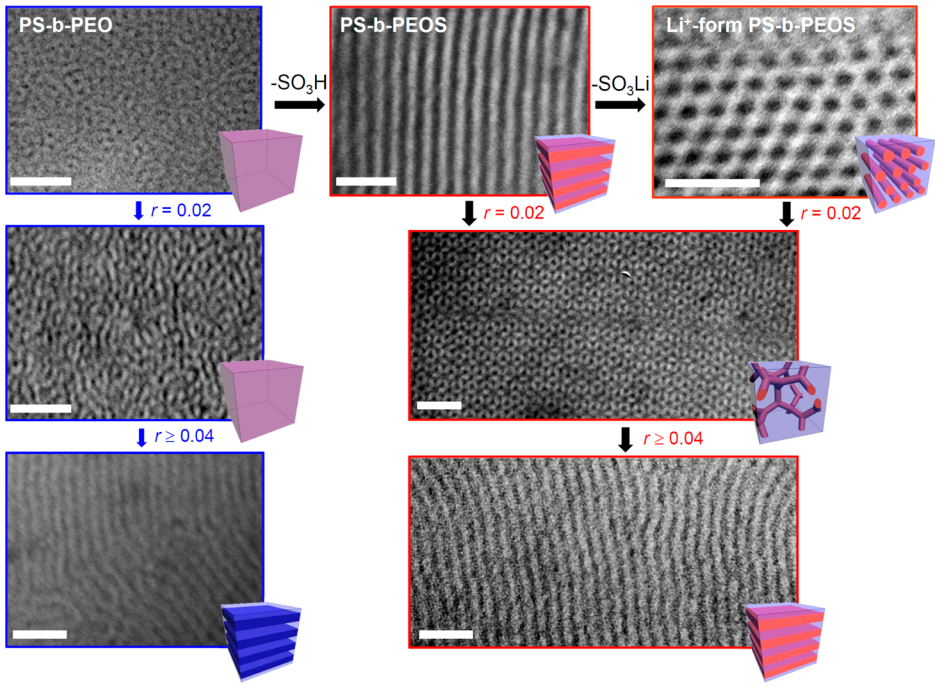

Figure 2. Transmission electron micrographs of PS-b-PEO and PS-b-PEOS obtained at different Li-salt concentrations, representing morphological variations associated with end-functional groups. Schematics given in the insets depict the type of self-assembled morphology. PEO (PEOS) phases were darkened by RuO_4 staining and the scale bars represent 50 nm.

functional terminal group substitution. A poly(styrene-*b*-ethylene oxide) (PS-b-PEO; 6.6−4.6 kg/mol) block copolymer was synthesized as a model polymer; variations in end groups of the model block copolymer were examined with respect to their self-assembled nanostructures and effects on conductivity. Challenges in obtaining well-defined morphologies and strategies for improving ion transport properties of the polymer electrolytes were elucidated. To the best of our knowledge, this is the first experimental report demonstrating the ability to tune the morphology and ion transport properties of bulk block copolymers by chain-end manipulation, without the need for other chemical alterations. We anticipate that the results described herein will be applicable to a wide range of emerging nanotechnologies ranging from separation membranes[27] and electrochemical devices,[28] to energy storage and conversion technologies.[29]

Two types of PS-b-PEO block copolymers having dissimilar end groups, that is, −OH and $-SO_3H$, were obtained by reaction with methanol and 1,3-propanesultone, respectively, during the termination step of anionic polymerization, as shown in Figure 1. Hereafter, PS-b-PEO represents the copolymer possessing −OH terminal groups and the $-SO_3H$-terminated PS-b-PEO block copolymer is referred to as PS-b-PEOS. Unreacted PS-b-PEO and 1,3-propanesultone in the preparation of PS-b-PEOS were removed by repeated precipitation and dialysis; ^{1}H NMR spectral analysis confirmed >99% sulfonic acid substitution on the PEO chains. A representative ^{1}H NMR spectrum of the PEOS chains is shown in Figure S1 (Supporting Information). Synthesis of the Li^+ form of PS-b-PEOS was then carried out by the reaction with excess of Li acetate, followed by purification using dialysis. The exchange efficiency was determined to be >99% by titration.

A set of transmission electron micrographs shown in Figure 2 illustrate the morphological variations of the PS-b-PEO block copolymers associated with the end-functional groups. The −OH terminated PS-b-PEO exhibited a poorly defined morphology, whereas the addition of a single $-SO_3H$ group to PS-b-PEO (i.e., PS-b-PEOS) resulted in the development of a lamellar (LAM) morphology. The appearance of an ordered

dx.doi.org/10.1021/mz400468m | *ACS Macro Lett.* 2013, 2, 990−995

morphology for PS-b-PEOS implies an increased effective Flory–Huggins interaction parameter (χ_{eff}) as a result of $-SO_3H$ attachment. This increase is attributed to an unfavorable interaction between the constituent blocks.[30] This is undoubtedly due to the increased incompatibility of PEOS phases with nonionic PS chains. On preparation of a Li^+ form PS-b-PEOS, we observed an intriguing morphological change from a LAM to hexagonal cylinder (HEX), in which the PEOS cylinders were dispersed in a PS matrix; this was indicative of a decreased PEOS phase volume upon replacing protons by Li^+ ions at the sulfonate chain end. We thus made a hypothesis that Li^+ ions at the terminal sulfonate groups eliminate the free volume created by hydrogen bonding that ultimately leads to the changes in packing properties of the PEO chains. This speculation will be further demonstrated through the following sections.

The preparation of Li-doped polymer electrolytes is essential for their practical use in lithium batteries, which has been shown to affect the self-assembly behavior of block copolymers.[18,31,32] A common conclusion from the body of literature on Li-salt-doped PS-b-PEO block copolymers is that the addition of a few percent of Li salt (represented as r = [Li^+]/[EO]) leads to an increment in the χ_{eff} value.[32−34] This phenomenon was also observed for our system; the disordered PS-b-PEO transformed into an ordered LAM morphology with 4% [Li][TFSI] (TFSI = $[(CF_3SO_2)_2N]^-$) doping (r = 0.04), as shown in Figure 2. Interestingly, a range of Li salt concentrations afforded enriched nanostructures adopted by the PS-b-PEOS block copolymer, which stand apart from a simple increase in the χ_{eff} value upon the addition of Li salts.

As shown in Figure 2, PS-b-PEOS, with a small degree of [Li][TFSI] doping (r = 0.02), exhibited a morphological transition from LAM to gyroid. If the increase in χ_{eff} was only arisen for the Li-salt-doped PS-b-PEOS, the anticipated microstructure progression would be LAM along a vertical trajectory of the well-established nonionic block copolymer phase diagram.[13] However, the development of gyroid morphology is indicative of an alteration in the volume fraction of PEOS phases (ϕ_{PEOS}) upon incorporation of [Li][TFSI] into the polymer, which is sufficiently large to cross the order-to-order phase boundaries. Given that cocontinuous channels of the gyroid structure were constructed by PEOS phases, it is inferred that the ϕ_{PEOS} decreased with the addition of [Li][TFSI]. Upon increasing [Li][TFSI] concentration to r = 0.06, the re-emergence of LAM morphology was observed, suggesting that the PEOS phases ultimately swell in the presence of a large amount of Li salt. It is worthwhile to note that analogous gyroid and LAM morphologies were seen for Li^+ form of PS-b-PEOS at the same [Li][TFSI] concentrations, that is, the occurrence of HEX-to-gyroid-to-LAM phase transitions.

Small-angle X-ray scattering (SAXS) experiments were carried out to further investigate the intriguing self-assembly behavior of PS-b-PEO block copolymer in relation to the nature of chain-end functionalization and Li-salt doping. The samples were laminated into an airtight sample cell to avoid the issue of water contamination. Representative SAXS profiles of PS-b-PEO and PS-b-PEOS block copolymers at different Li-salt concentrations obtained at 60 °C are shown in Figure 3a and b, respectively. Note that the profiles were unchanged in the temperature window of interest. As can be seen from Figure 3a, the PS-b-PEO showed a disordered-to-LAM phase transition with an increase in [Li][TFSI] loadings. In contrast, a range of

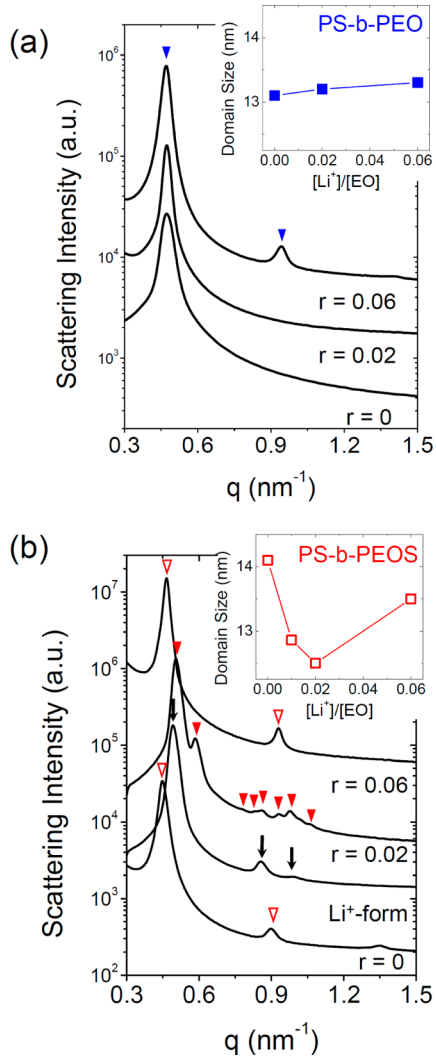

Figure 3. SAXS profiles of (a) PS-b-PEO and (b) PS-b-PEOS block copolymers at different [Li][TFSI] concentrations obtained at 60 °C. The inverted filled triangles (▼) in (a) indicate Bragg peaks at q^* and $2q^*$ for PS-b-PEO. The inverted open triangles (∇), the inverted filled triangles (▼), and the arrows (↓) in (b) represent Bragg peaks at q^*, $2q^*$; at $\sqrt{6}q^*$, $\sqrt{8}q$, $\sqrt{14}q^*$, $\sqrt{16}q^*$, $\sqrt{20}q^*$, $\sqrt{22}q^*$, $\sqrt{24}q^*$, $\sqrt{26}q^*$; and at q^*, $\sqrt{3}q^*$, $\sqrt{4}q^*$, respectively. The changes in domain spacing as a function of Li-salt concentration are plotted in the insets of (a) and (b).

ordered morphologies, that is, LAM, HEX, and gyroid, were observed for the PS-b-PEOS with a variation in Li salt concentration. The SAXS results are in excellent agreement with the transmission electron micrographs (Figure 2).

Notably, as plotted in the insets of Figure 3a,b, radical alterations in the domain size were accompanied by morphological transitions of PS-b-PEOS, in contrast to negligible changes in domain size seen for PS-b-PEO. First, the inclusion of a terminal $-SO_3H$ unit in PS-b-PEO caused a large increase in domain size from 13.1 to 14.1 nm. This observation is attributed to the formation of hydrogen bonds within the PEOS phases in PS-b-PEOS, which affects the packing density (molar volume) of PEO chains. X-ray diffraction (XRD) profiles demonstrating the inhibited crystallization of PEOS chains in PS-b-PEOS are shown in Figure S2 (Supporting Information). The differential scanning calorimetry (DSC) thermogram of PS-b-PEOS (Figure S3 of

dx.doi.org/10.1021/mz400468m | ACS Macro Lett. 2013, 2, 990−995

Supporting Information) displayed a significantly broadened melting peak at a melting temperature lower than that of PS-b-PEO. This is, in part, consistent with the results of Ohno et al. where the crystallization of PEO homopolymers was prevented by the replacement of terminal hydroxyl groups with sulfonate groups.[35]

When preparing the Li^+ form of PS-b-PEOS, a substantial reduction in domain size from 14.1 to 12.8 nm was observed, implying that a screening of hydrogen bonding results in a decrease in ϕ_{PEOS}. The value further decreased to 12.5 nm at r = 0.02 and was restored to 13.5 nm with an increase in [Li][TFSI] concentration to r = 0.06. It thus appears that at the low [Li][TFSI] concentrations, the sulfonate end groups effectively participated in attractive electrostatic interactions with Li^+ ions, thereby causing the decrease in ϕ_{PEOS}. Because the domain size of PS-b-PEOS became comparable to that of PS-b-PEO at high Li-salt loading, we inferred that an ample amount of Li^+ ions and $TFSI^-$ counterions were now free to distribute along the ether backbone. Thus, the thermodynamic effects of the terminal group on PS-b-PEOS are attenuated. Scheme 1 depicts the proposed dissimilar interchain interactions of the PEOS chains having sulfonate end groups. The internal sulfonate groups located near the PEO backbone could form hydrogen bonds, quadrupoles, and Li^+ coordination with the ether oxygen atoms, leading to dissimilar packing properties of PEOS chains. The Fourier transform infrared (FT-IR) spectra of PS-b-PEOS and the Li^+ form of PS-b-PEOS block copolymers (Figure 4S, Supporting Information) provide further indication of hydrogen bond screening upon the replacement of a proton by a Li^+ ion.

Scheme 1. Schematic Drawings of the Proposed Dissimilar Interchain Interactions of the PEOS Chains Having Sulfonate End Groups[a]

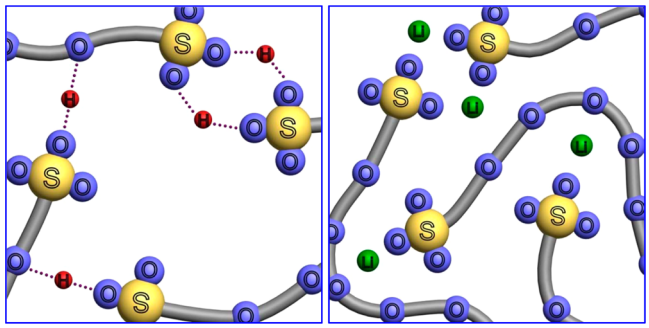

[a]The formation of hydrogen bonds (PS-b-PEOS) and quadrupoles and Li^+-coordination with ether oxygen atoms (Li^+-form PS-b-PEOS) resulted in dissimilar packing properties of the PEOS chains.

Next, we studied the effect of the charged end groups on the ionic conductivities of PS-b-PEO block copolymers. For low molecular weight PEO homopolymers having sulfonated groups at their chain ends (approximately 8−13 mol %), ion mobility was largely influenced by the nature of the end groups, as the ions were not equally distributed on all parts of the PEO chain, yielding considerable changes in chain dynamics.[35] Such effects may not present for the PS-b-PEOS block copolymer owing to the considerably lower sulfonate group content (as small as 1 mol %).

Figure 4 represents two sets of conductivity data, obtained using AC impedance spectroscopy at fixed Li^+ ion concentrations of r = 0.02 and 0.06. As can be seen in Figure 4a, at r = 0.02, the conductivity of the Li^+ form of PS-b-PEOS with gyroid morphology was qualitatively similar to that of disordered PS-b-PEO at low temperatures; however, the value noticeably surpassed that of PS-b-PEO when the temperature was increased above 65 °C. In contrast, at r = 0.06 (Figure 4b), the conductivity of the Li^+ form of the PS-b-PEOS copolymer with an analogous LAM morphology was lower than that of PS-b-PEO by about 60 ± 25% over the entire temperature window of interest. The slow segmental motion of Li^+ ion-complexed PEOS chains is inferred from the formation of internal sulfonate-based electrostatic interactions involving strong ionic pairs (aggregates) with Li^+ ion,[36,37] which are tied to the low conductivity. In this context, the high conductivity seen for gyroid-forming PS-b-PEOS is remarkable.

To elucidate the effect of morphology on ionic conductivity, the conductivity data shown in Figure 4a,b were normalized based on those of PEO (PEOS) homopolymers. The conductivity results of PEO and PEOS homopolymers utilized for the normalization are provided in Figure S5 of Supporting Information. We employed eq 1, given below,[38] where σ_{nor} is the normalized conductivity, σ_{block} is the conductivity of the Li-salt-doped block copolymer, and σ_{homo} is that of the homopolymer analog measured using 5 kg/mol PEO (PEOS) at a given Li-salt concentration:

$$\sigma_{nor} = \frac{\sigma_{block}}{\phi_{cond}\sigma_{homo}} \quad (1)$$

Here, ϕ_{cond} is the volume fraction of conducting PEO (PEOS) phases in PS-b-PEO (PS-b-PEOS). For PS-b-PEO, a fixed ϕ_{cond} value of 0.41, as calculated from the density and molecular weight of PS and non-Li-doped PEO, was used. Owing to the unknown density of PEOS in PS-b-PEOS, the ϕ_{cond} was estimated to be 0.42 ± 0.05 from TEM image analysis.

Figure 4c,d shows the σ_{nor} for PS-b-PEO and PS-b-PEOS in a temperature window of 50−90 °C (above the melting temperature of PEO chains) at Li^+ concentrations of r = 0.02 and 0.06. Strikingly, as shown in Figure 4c, when the morphologies of PS-b-PEO and PS-b-PEOS were deviated as disorder and gyroid, respectively, the σ_{nor} value of gyroid-forming PS-b-PEOS was revealed to be 2-fold higher than that of disordered PS-b-PEO. The substantially augmented Li^+ transport efficiency across the PEO domains is closely related to the structural advantages of gyroid possessing cocontinuous ionic channels, enabling the creation of less tortuous ion conduction pathways.[39] In contrast, at r = 0.06 (Figure 4d), a qualitatively similar σ_{nor} value was obtained for the LAM-forming PS-b-PEO and PS-b-PEOS block copolymers. It can thus be inferred that the type of self-assembled morphology has a profound impact on the respective ion transport efficiencies across ordered grains. It is also worthwhile to note here that σ_{nor} for various morphologies decreases in the order: gyroid > LAM > disordered.

It should be noted here that the σ_{nor} of the disordered sample given in Figure 4c could be undervalued to some extent given that we did not take into account the effects of PS chains on the glass transition temperature of the PEO phases.[19] We also anticipate that the degree of difference in σ_{nor} values probably will be weakened as the molecular weight of PEO chains is increased due to a decrease in end-group concentration.

Our results clearly demonstrate the unique ability to control the morphology of block copolymer electrolytes by attachment of a single end functional unit, which is the key to improving

dx.doi.org/10.1021/mz400468m | ACS Macro Lett. 2013, 2, 990−995

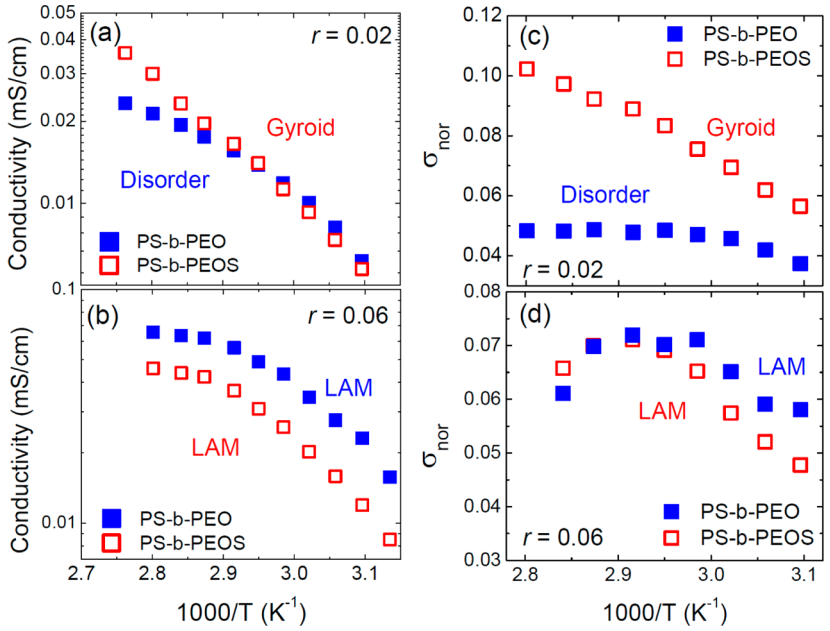

Figure 4. Temperature-dependent ionic conductivity and normalized conductivity (σ_{nor}) of PS-b-PEO (filled symbols) and PS-b-PEOS (open symbols) at r = 0.02 (a, c) and r = 0.06 (b, d). The type of self-assembled morphology is noted in the figure.

their ion transport efficiencies. While the absolute conductivity values obtained in the present study are low to be used in practical applications owing to the low Li-salt concentrations, the unprecedented, terminal-group-driven modulation of ion transport properties established in the present study will open new avenues for designing next-generation polymer electrolytes for various organic electronic devices.

In summary, we put forth a novel methodology for improving the ion transport properties of block copolymer electrolytes by the introduction of functional terminal groups. For PS-b-PEO block copolymers bearing sulfonate terminal groups, various self-assembled morphologies such as lamellae, hexagonal cylinder, and gyroid were obtained over a range of Li-salt concentrations, in accordance with radical changes in domain size. This was attributed to the modulation of specific intermolecular interactions in the ion-tethered PEO phases. Organization of the ion-conduction domains of block copolymers into self-assembled nanostructures proved beneficial for increasing ion transport rates. In particular, the ion transport efficiency could be largely enhanced if ordered, cocontinuous ionic channels were developed. The above results hold implications for the design of future polymer electrolytes, in which enhanced performances can be obtained through a precise control of their nanoscale morphologies by functional end group manipulation.

EXPERIMENTAL SECTION

Synthesis of PS-b-PEO, PS-b-PEOS, and the Li^+ Form PS-b-PEOS Block Copolymers. A poly(styrene-b-ethylene oxide) (PS-b-PEO) block copolymer (6.4−4.6 kg/mol) was synthesized by sequential anionic polymerization of styrene and ethylene oxide.[40] End-functionalized PS-b-PEO block copolymers were obtained by termination reaction with methanol and 1,3-propanesultone. The completion of the end functionalization was confirmed by ^{1}H NMR (Bruker AVB-300) spectroscopy. For the preparation of the Li^+ form of PS-b-PEOS, the PS-b-PEOS was dissolved as about 1 wt % in benzene and methanol mixtures (50/50 vol%). The 50× excess amount of Li acetate per moles of $-SO_3H$ was then added to the polymer solution. The mixture was stirred for 24 h and purified by dialysis in methanol. The exchange efficiency was determined as >99% by titration.

Morphology and Conductivity. The morphology of neat and Li-salt-doped block copolymers were characterized by combining cross-sectional transmission electron microscopy and synchrotron small-angle X-ray scattering experiments (4C beamline at the Pohang Light Source). In an Ar-filled glovebox, the through-plane conductivities of Li-salt-doped polymer membranes were measured using a two-electrode cell, where data were collected using a 1260 Solatron impedance analyzer.

ASSOCIATED CONTENT

Supporting Information

Additional information on the synthesis and characterization of the PS-b-PEO and PS-b-PEOS block copolymers. This material is available free of charge via the Internet at http://pubs.acs.org.

AUTHOR INFORMATION

Corresponding Author

*E-mail: moonpark@postech.edu.

Notes

The authors declare no competing financial interest.

ACKNOWLEDGMENTS

This work was financially supported by Midcareer Researcher Program (2012-0005267) and the Global Frontier R&D Program on Center for Multiscale Energy System funded by the National Research Foundation under the Ministry of Science, ICT & Future, Korea (2012-054173). We also acknowledge World Class University program funded by the Ministry of Education, Science and Technology through the National Research Foundation of Korea (R31-10059).

REFERENCES

(1) Wright, P. V. *Br. Polym. J.* **1975**, *7*, 319−327.
(2) Tarascon, J.-M.; Armand, M. *Nature* **2001**, *414*, 359−367.
(3) Trapa, P. E.; Huang, B. Y.; Won, Y. Y.; Sadoway, D. R.; Mayes, A. M. *Electrochem. Solid State* **2002**, *5*, A85−A88.

(4) Soo, P. P.; Huang, B. Y.; Jang, Y. I.; Chiang, Y. M.; Sadoway, D. R.; Mayes, A. M. *J. Electrochem. Soc.* **1999**, *146*, 32−37.
(5) Singh, M.; Odusanya, O.; Wilmes, G. M.; Eitouni, H. B.; Gomez, E. D.; Patel, A. J.; Chen, V. L.; Park, M. J.; Fragouli, P.; Iatrou, H.; Hadjichristidis, N.; Cookson, D.; Balsara, N. P. *Macromolecules* **2007**, *40*, 4578−4585.
(6) Wang, C. X.; Sakai, T.; Watanabe, O.; Hirahara, K.; Nakanishi, T. *J. Electrochem. Soc.* **2003**, *150*, A1166−A1170.
(7) Niitani, T.; Shimada, M.; Kawamura, K.; Dokko, K.; Rho, Y. H.; Kanamura, K. *Electrochem. Solid State Lett.* **2005**, *8*, A385−A388.
(8) Trapa, P. E.; Won, Y. Y.; Mui, S. C.; Olivetti, E. A.; Huang, B. Y.; Sadoway, D. R.; Mayes, A. M.; Dallek, S. *J. Electrochem. Soc.* **2005**, *152*, A1−A5.
(9) Cho, B.-K.; Jain, A.; Gruner, S. M.; Wiesner, U. *Science* **2004**, *305*, 1598−1601.
(10) Itoh, T.; Ikeda, M.; Hirata, N.; Moriya, Y.; Kubo, M.; Yamamoto, O. *J. Power Sources* **1999**, *81/82*, 824−829.
(11) Ghosh, A.; Wang, C.; Kofinas, P. *J. Electrochem. Soc.* **2010**, *157*, A846−A849.
(12) Kim, O.; Jo, G.; Park, Y. J.; Park, M. J. *J. Phys. Chem. Lett.* **2013**, *4* (13), 2111−2117.
(13) Bates, F. S.; Fredrickson, G. H. *Phys. Today* **1999**, *52*, 32−38.
(14) Epps, T. H.; Bailey, T. S.; Waletzko, R.; Bates, F. S. *Macromolecules* **2003**, *36*, 2873−2881.
(15) Floudas, G.; Vazaiou, B.; Schipper, F.; Ulrich, R.; Wiesner, U.; Iatrou, H.; Hadjichristidis, N. *Macromolecules* **2001**, *34*, 2947−2957.
(16) Ryan, A. J.; Mai, S.-M.; Fairclough, J. P. A.; Hamley, I. W.; Booth, C. *Phys. Chem. Chem. Phys.* **2001**, *3*, 2961−2971.
(17) Gomez, E. D.; Panday, A.; Feng, E. H.; Chen, V.; Stone, G. M.; Minor, A. M.; Kisielowski, C.; Downing, K. H.; Borodin, O.; Smith, G. D.; Balsara, N. P. *Nano Lett.* **2009**, *9*, 1212−1216.
(18) Wanakule, N. S.; Panday, A.; Mullin, S. A.; Gann, E.; Hexemer, A.; Balsara, N. P. *Macromolecules* **2009**, *42*, 5642−5651.
(19) Yuan, R.; Teran, A. A.; Gurevitch, I.; Mullin, S. A.; Wanakule, N. S.; Balsara, N. P. *Macromolecules* **2013**, *46*, 914−921.
(20) Teran, A. A.; Mullin, S. A.; Hallinan, D. T.; Balsara, N. P. *ACS Macro Lett.* **2012**, *1*, 305−309.
(21) Choi, I.; Ahn, H.; Park, M. J. *Macromolecules* **2011**, *44*, 7327−7334.
(22) Kim, J. K.; Kim, M. I.; Kim, H. J.; Lee, D. H.; Jeong, U.; Jinna, H.; Suda, K. *Macromolecules* **2007**, *40*, 7590−7593.
(23) Sotiroiu, K.; Pispas, S.; Hadjichristidis, N. *Macromol. Chem. Phys.* **2004**, *205*, 55−62.
(24) Liu, J. S.; Tanaka, T.; Sivula, K.; Alivisatos, A. P.; Fréchet, J. M. J. *J. Am. Chem. Soc.* **2004**, *126*, 6550−6551.
(25) Huh, J.; Jung, J. Y.; Lee, J. U.; Cho, H.; Park, S.; Park, C.; Jo, W. H. *ACS Nano* **2011**, *5*, 155−122.
(26) Willcock, H.; O'Reilly, R. K. *Polym. Chem* **2010**, *1*, 149−157.
(27) Phillip, W. A.; O'Neill, B.; Rodwogin, M.; Hillmyer, M. A.; Cussler, E. L. *ACS Appl. Mater. Interfaces* **2010**, *2*, 847−853.
(28) Lindner, S. M.; Hüttner, S.; Chiche, A.; Thelakkat, M.; Krausch, G. *Angew. Chem., Int. Ed.* **2006**, *45*, 3364−3368.
(29) Park, M. J.; Choi, I.; Hong, J.; Kim, O. *J. Appl. Polym. Sci.* **2013**, *129*, 2363−2376.
(30) Park, M. J.; Balsara, N. P. *Macromolecules* **2008**, *41*, 3678−3687.
(31) Young, W.-S.; Epps, T. H. *Macromolecules* **2009**, *42*, 2672−2678.
(32) Wanakule, N. S.; Virgili, Z. M.; Teran, A. A.; Wang, Z.-G.; Balsara, N. P. *Macromolecules* **2010**, *43*, 8282−8289.
(33) Nakamura, I.; Wang, Z.-G. *Soft Matter* **2012**, *8*, 9356−9367.
(34) Nakamura, I.; Balsara, N. P.; Wang, Z.-G. *ACS Macro Lett.* **2012**, *1*, 305−309.
(35) Ito, K.; Nishina, N.; Ohno, H. *J. Mater. Chem.* **1997**, *7*, 1357−1362.
(36) Fragiadakis, D.; Dou, S.; Colby, R. H.; Runt, J. *Macromolecules* **2008**, *41*, 5723−5728.
(37) Wang, W.; Liu, W.; Tudryn, G. J.; Colby, R. H.; Winey, K. I. *Macromolecules* **2010**, *43*, 4223−4229.
(38) Kim, O.; Kim, Jo, G.; Park, Y.; Kim, S.; Park, M. J. *J. Phys. Chem. Lett.* **2013**, *4*, 2111−2117.
(39) Kim, O.; Kim, S. Y.; Ahn, H.; Kim, C. W.; Rhee, Y. M.; Park, M. J. *Macromolecules* **2012**, *45*, 8702−8713.
(40) Hadjichristidis, N.; Iatrou, H.; Pispas, S.; Pitsikalis, M. *J. Polym. Sci., Polym. Chem.* **2000**, *38*, 3211−3234.